Mon. Not. R. Astron. Soc. **000**, 1–15 (?) Printed 8 February 2022 (MN LATEX style file v2.2)

Modelling spin-up episodes in accreting millisecond X-ray pulsars

Kostas Glampedakis[1,2⋆] and Arthur G. Suvorov[2,3]†
[1] *Departamento de Física, Universidad de Murcia, Murcia, E-30100, Spain*
[2] *Theoretical Astrophysics, Eberhard Karls University of Tübingen, Tübingen, D-72076, Germany*
[3] *Manly Astrophysics, 15/41-42 East Esplanade, Manly, NSW 2095, Australia*

arXiv:2109.07657v1 [astro-ph.HE] 16 Sep 2021

Accepted ?. Received ?; in original form ?

ABSTRACT

Accreting millisecond X-ray pulsars are known to provide a wealth of physical information during their successive states of outburst and quiescence. Based on the observed spin-up and spin-down rates of these objects it is possible, among other things, to infer the stellar magnetic field strength and test models of accretion disc flow. In this paper we consider the three accreting X-ray pulsars (XTE J1751–305, IGR J00291+5934 & SAX J1808.4–3658) with the best available timing data, and model their observed spin-up rates with the help of a collection of standard torque models that describe a magnetically-threaded accretion disc truncated at the magnetospheric radius. Whilst none of these models are able to explain the observational data, we find that the inclusion of the physically motivated phenomenological parameter ξ, which controls the uncertainty in the location of the magnetospheric radius, leads to an enhanced disc-integrated accretion torque. These 'new' torque models are compatible with the observed spin-up rates as well as the inferred magnetic fields of these objects provided that $\xi \approx 0.1 - 0.5$. Our results are supplemented with a discussion of the relevance of additional physics effects that include the presence of a multipolar magnetic field and general-relativistic gravity.

Key words: stars: neutron, magnetic fields, X-rays: binaries, accretion

1 INTRODUCTION

Accreting neutron stars in low mass X-ray binaries (LMXBs) rank amongst the most well-studied compact objects in astrophysics. Interactions between the neutron star's strong magnetic field and general-relativistic (GR) gravity with the freely falling plasma accretion flow from the companion star can spin-up the neutron star to $\gtrsim$ millisecond rotation periods and provide fuel that can ignite atop the stellar surface, triggering thermonuclear explosions (Galloway & Keek 2021). As such, the rich physical environment of LMXBs can be used to study neutron star phenomenology in a variety of ways. For instance, the properties of X-ray flashes from bursting LMXBs (Li et al. 1999; Güver & Özel 2013), and of thermal relaxation (Page & Reddy 2013; Potekhin & Chabrier 2018) or emissions (Bogdanov et al. 2019; Miller et al. 2021) from quiescent systems, lead to measurements of local (e.g., crust microphysics) and global (e.g., mass-radius) quantities that are subsequently converted into constraints for the equation of state of neutron star matter (Lattimer & Prakash 2001). Mapping out the spin-temperature plane of LMXBs additionally allows one to study the intricate excitation and quenching mechanisms (Ho, Andersson & Haskell 2011; Strohmayer & Mahmoodifar 2014) of the gravitational wave-driven r-mode instability (Andersson, Kokkotas & Stergioulas 1999). Gravitational wave (GW) emissions from LMXBs could additionally take place as a result of the transient formation of quadrupolar 'mountains' and may be responsible for the observed spin-down irregularities (Haskell & Patruno 2017). The physics of LMXB accretion discs and magnetic fields – the focus of this paper – may also be revealed via quasi-periodic oscillations (van der Klis 2006), emission lines (Cackett et al. 2009), and spin-up observations.

A particularly important subpopulation of LMXBs comprises the accreting millisecond X-ray pulsars (AMXPs) [see Patruno & Watts (2021) for a review]; these systems emit X-ray pulses energised by the plasma captured from the accretion disc and channeled onto the neutron star's magnetic poles. The emission is modulated by the neutron star's rotation, thus allowing a precision measurement of the spin

⋆ kostas@um.es
† arthur.suvorov@tat.uni-tuebingen.de

© ? RAS

frequency. The hypothesised link between accreting neutron stars and the older population of recycled millisecond pulsars (Alpar et al. 1982; Bhattacharya & van den Heuvel 1991) was confirmed by the discovery of the first AMXP in 1998 (Wijnands & van der Klis 1998) and the 'swinging' pulsars IGR J18245–2452 and PSR J1023+2038, which alternate between radio- and X-ray loud states, some years later (Archibald et al. 2009; Papitto et al. 2013). Indeed, AMXPs could hardly be classified as steady-state systems; their accretion lifetime is punctuated by active phases during which a markedly increased mass accretion rate (which stands as a proxy for the observed X-ray luminosity) leads to a spin-up episode via the action of the accretion disc's torque. In between these episodes, the system accretes at a much lower rate (which may involve a tenuous receding inner disc) and the spin evolution in this state of quiescence is expected to be dominated by the star's own electromagnetic spin-down torque (Gunn & Ostriker 1969).

Much work has been dedicated to the study of the long-term, time-averaged spin equilibrium frequency of AMXPs (and of other LMXBs with known spin periods). Early models invoked a GW-accretion torque balance (Bildsten 1998; Levin 1999; Andersson et al. 2000) but subsequent work has shown that magnetic coupling to the accretion disc may be the key mechanism for spin equilibrium (Rappaport, Fregeau & Spruit 2004; Andersson et al. 2005; Bhattacharyya & Chakrabarty 2017). More relevant to the present work is the theoretical modelling of spin-up episodes in AMXPs as observed during active outburst periods. Two of these systems, XTE J1751–305 and IGR J00291+5934, were studied by Andersson, Jones & Ho (2014) with the help of standard accretion torque models available in the literature. They found that these torques fall short of explaining the spin-up and magnetic field data, thus casting some doubt on our understanding of the physics of these systems.

In this paper we revisit the topic of accretion spin-up in AMXPs by performing a systematic study of those three systems, XTE J1751–305, IGR J00291+5934 & SAX J1808.4–3658, which currently have the best-measured spin evolution during outburst and quiescent phases. We provide a detailed discussion of the data and the associated observational and systematic uncertainties, and highlight some physical differences between the various sources. In the first part of the paper the spin-up torques are modelled within the framework of standard accretion theory, where the disc is coupled to the stellar magnetic field and is truncated at the magnetospheric radius. The new aspect of our approach, not considered by earlier work, lies in the incorporation of the phenomenological parameter ξ as a measure of the uncertain physics in the vicinity of the magnetospheric radius. For the physically motivated case where $\xi < 1$, we find that models which account for magnetic field threading of the disc can lead to spin-up rates comparable to the observational data whilst being consistent with the inferred magnetic field from the spin-down data. This is the main result of this paper. The second part of our analysis consists of a quantitative discussion of what we consider to be the most important 'additional physics' corrections to the basic model, namely, a magnetic field which is not purely dipolar and some key effects of GR gravity.

The rest of the paper is organised as follows. In Sections 2.1-2.2 we discuss the various accretion torque models available in the literature and construct two 'new' ones, which are then compared in Section 2.3. In Section 2.4 we discuss the constraints imposed on the magnetic field by the geometry of the accretion disc. The necessary spin evolution formulae are presented in Section 2.5. Section 3 is the main part of this paper and contains the comparison of the theoretical accretion torques against the observed spin-up episodes of three AMXPs with reliable timing data (Sections 3.2-3.4). In Section 4 we resume our theoretical discussion of accretion physics by considering the effect of a multipolar stellar magnetic field (Section 4.1) and of GR gravity (Sections 4.2-4.3). Our concluding remarks can be found in Section 5. The Appendix contains some secondary technical details related to the structure of the standard accretion disc model.

Notation: Throughout the paper we use a star symbol to label stellar parameters. Moreover, we adopt the following fairly standard normalisations for the stellar mass $M_\star$, radius $R_\star$, and (dipole) polar field strength $B_\star$: $M_{1.4} = M_\star/1.4\,M_\odot$, $R_6 = R_\star/10^6\,\mathrm{cm}$, and $B_8 = B_\star/10^8\,\mathrm{G}$. In addition, the stellar spin frequency $\nu_\star$, accretion rate $\dot{M}$, and X-ray luminosities L_X are normalised as $\nu_{500} = \nu_\star/500\,\mathrm{Hz}$, $\dot{M}_{-10} = \dot{M}/10^{-10} M_\odot \mathrm{yr}^{-1}$, and $L_{\mathrm{X},36} = L_\mathrm{X}/10^{36}\ \mathrm{erg\ s}^{-1}$, respectively.

2 MODELS OF ACCRETION TORQUES

This theoretical first part of the paper provides a detailed survey of the various analytical accretion torque models available in the market. As discussed below, these are largely phenomenological constructions that correspond to different viable choices for the disc's truncation radius and its interaction with the stellar magnetic field. Using the same logic, we add one more model to this torque collection and then go on to compare these models against observed spin-up episodes of AMXPs.

2.1 Baseline accretion torque model with a magnetic field

In what could be called the 'standard accretion torque model' the disc is assumed to be geometrically thin and quasi-stationary over timescales much longer than the hydrodynamical and orbital timescales of the accreted matter. The interaction of the stellar magnetic field with the disc is assumed to fall well within the domain of the usual magnetohydrodynamic (MHD) framework. In addition, this baseline model assumes Newtonian gravity (the impact of GR gravity is discussed in a later section) and axisymmetry with respect to the stellar spin axis.

The disc's 'equation of motion' (in standard cylindrical coordinates $\{r, \varphi, z\}$) is the following thickness-integrated Euler equation [cf. Ghosh & Lamb (1979), Rappaport, Fregeau & Spruit (2004)],

$$-\dot{M}\frac{d}{dr}\left[\Omega(r) r^2\right] = B_z B_\varphi r^2 + \mathcal{T}_\mathrm{visc}, \tag{1}$$

where $\Omega(r)$ is the disc's rotational profile and $\mathcal{T}_\mathrm{visc}$ is the viscous torque. The magnetic torque exerted on the disc by the stellar field comprises the poloidal and toroidal field

components, B_z and B_φ respectively. The magnetic field is assumed dipolar (this assumption is relaxed in a later section where we include higher magnetic multipole moments),

$$B_z = -B_\star \left(\frac{R_\star}{r}\right)^3 = -\frac{\mu_\star}{r^3}, \tag{2}$$

where $B_\star$ is the surface polar field and $\mu_\star$ is the corresponding dipole moment.

The magnetic field is likely to play an important dynamical role during accretion and dominate the flow below a 'magnetospheric' (or Alfvén) radius $R_{\rm m}$. The ensuing physical picture is that of a disc truncated in the region $r \approx R_{\rm m}$ with accreted matter being entirely channeled along the field lines and onto the polar caps (note, however, that the situation may be far more complex for a 'weak' magnetic field). Across the same region the angular frequency Ω is assumed to make a smooth transition from a Keplerian profile, $\Omega_{\rm K}(r) = \sqrt{GM_\star/r^3}$, to the stellar angular frequency, $\Omega_\star$ (Rappaport, Fregeau & Spruit 2004).

The magnetospheric radius is the first key lengthscale of the present accretion model. It is common practice in the literature to estimate this parameter based on the assumption of comparable energy densities for the orbiting gas and the (poloidal) magnetic field in the disc's truncation region (Frank, King & Raine 2002). If we define as $R_{\rm A}$ the resulting solution for $R_{\rm m}$, we have

$$\frac{1}{2}\rho\Omega_{\rm K}^2 R_{\rm A}^2 \approx \frac{B_z^2}{8\pi}. \tag{3}$$

When combined with standard thin disc structure equations (these are listed in Appendix A) this relation leads to,

$$R_{\rm A} \approx \xi \frac{\mu_\star^{4/7}}{\dot{M}^{2/7}(GM_\star)^{1/7}}. \tag{4}$$

This calculation's phenomenological parameter ξ is defined as,

$$\xi = (6\pi\alpha)^{2/7}\left(\frac{H}{R_{\rm A}}\right)^{6/7} \approx 0.2\left(\frac{\alpha}{0.1}\right)^{2/7}\left(\frac{H/R_{\rm A}}{0.1}\right)^{6/7}, \tag{5}$$

where in the second equation we have normalised the disc's thickness H and viscosity parameter α to their 'canonical' values. To some extent this parameter is a measure of our ignorance of the complicated physics taking place in the vicinity of the disc's truncation radius and it is typically assumed to vary within a range $\xi \approx 0.1 - 1$ (see also below). For $R_{\rm A}$ itself we obtain the numerical estimate,

$$R_{\rm A} \approx 35\,\xi\,\dot{M}_{-10}^{-2/7} M_{1.4}^{-1/7} R_6^{12/7} B_8^{4/7} \ \text{km}. \tag{6}$$

Alternatively, the magnetospheric radius can be obtained via a direct application of Eq. (1), after setting $\mathcal{T}_{\rm visc} \approx 0$ at the disc's truncation radius and approximating $d[\Omega r^2]/dr \approx \Omega_{\rm K} R_{\rm A}^2/\Delta r_{\rm m}$ where $\Delta r_{\rm m}$ is the radial width of the truncation (Psaltis & Chakrabarty 1999). The outcome of this calculation resembles Eq. (4) with

$$\xi = \left(\lambda_B \frac{\Delta r_{\rm m}}{R_{\rm A}}\right)^{2/7}, \qquad \lambda_{\rm B} \equiv \left|\frac{B_\phi}{B_z}\right|_{R_{\rm A}}. \tag{7}$$

Psaltis & Chakrabarty (1999) assume $\lambda_{\rm B} \sim 1$ and estimate $\Delta r_{\rm m}/R_{\rm A} \sim 0.01 - 1$ which translates to $\xi \approx 0.3 - 1$.

The two preceding (approximate) calculations clearly show that the ξ parameter lumps together uncertainties related to the disc structure as well as the relative poloidal-toroidal magnetic field strength in the vicinity of the magnetospheric radius.

The second key lengthscale of any accretion torque model is the so-called corotation radius $R_{\rm co}$, defined as the radial distance where the orbital and stellar frequencies match, i.e. $\Omega_\star = \Omega_{\rm K}(R_{\rm co})$. From this we easily find,

$$R_{\rm co} \approx 27\, M_{1.4}^{1/3} \nu_{500}^{-2/3} \ \text{km}. \tag{8}$$

Based on the above estimates we should expect $R_{\rm A} \sim R_{\rm co}$.

The truncation of the disc at $r \approx R_{\rm A}$ is associated with a 'material' Alfvén torque of increased lever-arm length (as compared to that of a non-magnetic system) (Pringle & Rees 1972),

$$N_{\rm A} = \dot{M} R_{\rm A}^2 \Omega_{\rm K}(R_{\rm A}) = \dot{M}\sqrt{GM_\star R_{\rm A}}. \tag{9}$$

Field lines rotating faster than the local Keplerian speed produce a negative torque and may lead to a propeller effect when $R_{\rm A} > R_{\rm co}$. In this regime the accretion flow will be centrifugally inhibited and matter may be ejected from the system [though see also Spruit & Taam (1993)]. As accreting matter is flung away, the star would experience a spin-down torque. A simple way to account for this effect is by modifying the previous torque (Andersson et al. 2005; Andersson, Jones & Ho 2014),

$$N_{\rm m} = \dot{M} R_{\rm A}^2 [\,\Omega_{\rm K}(R_{\rm A}) - \Omega_\star\,] = N_{\rm A}\,(1 - \omega_{\rm A})\,, \tag{10}$$

where we have introduced the so-called (dimensionless) fastness parameters,

$$\omega_{\rm A} \equiv x_{\rm A}^{3/2}, \qquad x_{\rm A} \equiv \frac{R_{\rm A}}{R_{\rm co}}. \tag{11}$$

The phenomenological expression (10) predicts spin equilibrium, $N_{\rm m} = 0$, to take place at $x_{\rm A} = 1$ in accordance with the intuitive picture described above. This equality translates to the following equilibrium spin frequency,

$$\nu_{\rm eq} \approx 283\,\xi^{-3/2} B_8^{-6/7} R_6^{-18/7} \dot{M}_{-10}^{3/7} M_{1.4}^{5/7} \ \text{Hz}, \tag{12}$$

which is in good agreement with the average spin frequency of the known LMXB population [see e.g., Patruno, Haskell & Andersson (2017)].

2.2 Accretion torque with a magnetically-threaded disc

We can raise the sophistication level of the preceding baseline model by taking into account the magnetic field-disc coupling and the ensuing wind-up of the field lines by the orbiting matter (Ghosh & Lamb 1979; Wang 1995). The generated toroidal field is described by the induction equation,

$$\partial_t B_\varphi = |\boldsymbol{\nabla} \times (\mathbf{v} \times \mathbf{B})|_\varphi. \tag{13}$$

This equation can be analytically handled by approximating $\partial_t B_\varphi \approx B_\varphi/\tau_\varphi$ and $\mathbf{v} = [\Omega_{\rm K}(r) - \Omega_\star]\hat{\boldsymbol{\varphi}}$. The physics behind the timescale τ_φ is somewhat sketchy; following Wang (1995) (which provides the most detailed analysis on the subject) we can parametrise the toroidal field as

$$B_\varphi(r) = \zeta B_z(r) f[\Omega_\star/\Omega_{\rm K}(r)], \tag{14}$$

where ζ is yet another phenomenological constant parameter. The function f depends on the mechanism responsible

for limiting the growth of B_φ; for turbulent diffusion in the disc ('mechanism (2)') and magnetic reconnection outside the disc ('mechanism (3)') Wang (1995) gives:

$$f_{(2)} = \frac{\Omega_\star}{\Omega_{\rm K}} - 1, \quad f_{(3)} = \begin{cases} f_{(2)}, & r < R_{\rm co} \\ \\ 1 - \Omega_{\rm K}/\Omega_\star, & r > R_{\rm co} \end{cases} \tag{15}$$

According to both prescriptions the toroidal field is generated in the prograde (retrograde) direction for $R < R_{\rm co}$ ($R > R_{\rm co}$).

As a result of the magnetic field lines threading the disc there is an additional accretion torque $N_{\rm disc}$ exerted on the neutron star. This is given by the integral[1],

$$N_{\rm disc} = -\int_{R_{\rm m}}^{\infty} dr r^2 B_\varphi B_z. \tag{16}$$

For the two toroidal field choices (15) we find

$$N^{(2)}_{\rm disc} = \frac{\zeta \mu_\star^2}{3R_{\rm m}^3}\left(1-2\omega\right), \tag{17}$$

$$N^{(3)}_{\rm disc} = \frac{\zeta \mu_\star^2}{9R_{\rm m}^3}\left(3-6\omega+2\omega^2\right), \tag{18}$$

where we have defined a new pair of fastness parameters,

$$\omega \equiv x^{3/2}, \quad x \equiv \frac{R_{\rm m}}{R_{\rm co}}, \tag{19}$$

The total accretion torque is the sum of the disc-integrated torque $N_{\rm disc}$ and the material torque at $r = R_{\rm m}$. This is given by the earlier baseline expressions (9), (10) with $R_{\rm A}$ replaced by a general $R_{\rm m}$ magnetospheric radius.

The reason we have allowed for the possibility of $R_{\rm m} \neq R_{\rm A}$ in this section is that Eq. (15), in combination with the assumption $\Omega(r) = \Omega_{\rm K}(r)$, allows the Euler equation (1) to become a relation for $R_{\rm m}$,

$$R_{\rm m} = (2\zeta)^{2/7} \frac{\mu_\star^{4/7}}{\dot{M}^{2/7}(GM_\star)^{1/7}} \left[1 - \left(\frac{R_{\rm m}}{R_{\rm co}}\right)^{3/2}\right]^{2/7}. \tag{20}$$

As is evident, this expression is self-consistent provided $R_{\rm m} < R_{\rm co}$. Moreover, it reduces to the earlier Alfvén radius (4), for $R_{\rm m} \ll R_{\rm co}$ and $\xi \to (2\zeta)^{2/7}$.

With this identification between phenomenological parameters, we can rewrite (20) as

$$x = x_{\rm A}\left(1-\omega\right)^{2/7}, \tag{21}$$

and we can see that apart from $x \leqslant 1$ we should also expect $x < x_{\rm A}$ (i.e. $R_{\rm m} < R_{\rm A}$).

The above torques and magnetospheric radii are combined in different ways in different papers in the literature. For example, in Wang (1995) the total torque is given by,

$$N^{\rm W(2,3)}_{\rm tot} = \dot{M}\sqrt{GM_\star R_{\rm m}} + N^{(2,3)}_{\rm disc}, \tag{22}$$

which with the further input of (21) leads to,

$$N^{\rm W(2)}_{\rm tot} = \frac{1}{3}N_{\rm A}\frac{(7/2-4\omega)}{(1-\omega)^{6/7}}, \tag{23}$$

$$N^{\rm W(3)}_{\rm tot} = \frac{1}{3}N_{\rm A}\frac{\left[\,7/2-4\omega+(1/3)\omega^2\,\right]}{(1-\omega)^{6/7}}. \tag{24}$$

These total torques predict spin equilibrium at

$$x^{(2)}_{\rm eq} \approx 0.91, \qquad x^{(3)}_{\rm eq} \approx 0.97. \tag{25}$$

Andersson et al. (2005) adopt the magnetospheric radius of Eqs. (20), (21) but opt for the material torque (10) in combination with the mechanism (2) disc torque. The resulting total torque is,

$$N^{\rm A}_{\rm tot} = \dot{M}\sqrt{GM_\star R_{\rm m}}(1-\omega) + N^{(2)}_{\rm disc} \tag{26}$$

$$= \frac{1}{3}N_{\rm A}\frac{\left(\,7/2-7\omega+3\omega^2\,\right)}{(1-\omega)^{6/7}}. \tag{27}$$

The corresponding spin equilibrium is found to be,

$$x^{\rm A}_{\rm eq} \approx 0.81. \tag{28}$$

Finally, Rappaport, Fregeau & Spruit (2004) and Bhattacharyya & Chakrabarty (2017) use the mechanism (3) torque of Wang (1995) with $\zeta = 1$ but deviate from that model by adopting the magnetospheric radius $R_{\rm m} = R_{\rm A}$ of the baseline model with $\xi = 1$. The resulting torque is,

$$N^{\rm R,BC}_{\rm tot} = N_{\rm A} + N^{(3)}_{\rm disc} = \frac{2}{3}N_{\rm A}\left(2-\omega_{\rm A}+\frac{1}{3}\omega_{\rm A}^2\right). \tag{29}$$

In contrast to the previous cases this torque does *not* admit a point of equilibrium.

It is straightforward to invent two 'new' torque models based on the above mechanism (2) & (3) prescription and by choosing $R_{\rm m} = R_{\rm A}$ *without* assuming $\xi = 1$. The first of these torques generalises expression (29),

$$N^{\rm new(3)}_{\rm tot} = \frac{2}{3}\xi^{-7/2}N_{\rm A}\left(\frac{1+3\xi^{7/2}}{2}-\omega_{\rm A}+\frac{1}{3}\omega_{\rm A}^2\right). \tag{30}$$

This torque vanishes at

$$\omega^{\rm new(3)}_{\rm A,eq} = \frac{3}{2}\left(1-\sqrt{\frac{1-6\xi^{7/2}}{3}}\right), \tag{31}$$

which is real-valued for $\xi < \xi_{\rm max} \approx 0.6$. If we assume $0.1 < \xi < \xi_{\rm max}$, the corresponding equilibrium x-point lies within the range,

$$0.74 \lesssim x^{\rm new(3)}_{\rm A,eq} \lesssim 1.3. \tag{32}$$

The second new torque is

$$N^{\rm new(2)}_{\rm tot} = \frac{1}{3}\xi^{-7/2}N_{\rm A}\left(1+3\xi^{7/2}-2\omega_{\rm A}\right), \tag{33}$$

and the associated equilibrium fastness parameter is

$$\omega^{\rm new(2)}_{\rm A,eq} = \frac{1}{2}\left(1+3\xi^{7/2}\right). \tag{34}$$

For the $0.1 < \xi < 1$ range this result returns,

$$0.63 < x^{\rm new(2)}_{\rm A,eq} \lesssim 1.6. \tag{35}$$

We can notice that both new models can accommodate $R_{\rm A} > R_{\rm co}$ (i.e. the propeller regime of the baseline model) as a viable spin-up regime.

[1] Strictly speaking, the integral's upper limit should be set at the light cylinder radius, $R_{\rm lc} = c/\Omega_\star \approx 96\,\nu_{500}$ km, which marks the separatrix of the last closed magnetic field line. However, the error introduced by taking the integral out to infinity is negligible given that $R_{\rm m}, R_{\rm co} \ll R_{\rm lc}$.

2.3 Comparing the various torques

None of the previous torques can be classified as 'rigorous' but, nevertheless, they do represent the state-of-the-art when it comes to modelling the spin evolution of accreting neutron stars. Among the models discussed we should expect those with a magnetically-threaded disc to be the most realistic ones. The situation is less clear when choosing[2] between $R_{\rm A}$, Eq. (4), or $R_{\rm m}$, Eq. (20). The first expression is the most widely used in the literature, although typically served with $\xi = 1$ which, in face of the estimate (5), may not be fully justified. Meanwhile, the assumption of a Keplerian angular frequency in the derivation of Eq. (20) may be equally unrealistic.

To some extent this discussion boils down to choosing the unknown function in the Euler equation (1). As we have seen, this equation can be approximated with respect to Ω and B_φ and solved for $R_{\rm m} = R_{\rm A}$ (Psaltis & Chakrabarty 1999); it can be solved for $R_{\rm m}$ assuming $\Omega = \Omega_{\rm K}$ and a specific functional form for $B_\varphi(r)$ (Wang 1995); it can be solved for $\Omega(r)$ for a given functional form $B_\varphi(r)$ and $R_{\rm m} = R_{\rm A}$ or for the viscous stress $\mathcal{T}_{\rm visc}(r)$ after assuming a Keplerian angular frequency (Kluźniak & Rappaport 2007).

As an executive summary, the various accretion torques that have been suggested in the literature (plus the ones discussed here) are listed in Table 1. Their relative strength (normalised to $N_{\rm A}$) as a function of the fastness parameter x (or $x_{\rm A}$) is shown in Fig. 1. We can see that among the previously used torque models, $N_{\rm tot}^{\rm R,BC}$ is the dominant one across the entire fastness parameter range. But the most prominent feature in this plot is the enhanced strength of the pair of 'new' torques as a result of the $\xi < 1$ degree of freedom. In particular, the enhancement originates from the negative ξ-power dependence of the disc-integrated portion $N_{\rm disc}$ of the torque rather than the material part $N_{\rm A}$.

It is worth pointing out that our discussion of the various torque models presented in Table 1 may be of some interest to the still open question of the spin distribution of AMXPs. The suggested separation in 'fast' and 'slow' subpopulations (Patruno, Haskell & Andersson 2017) could reflect the operation of different torque mechanisms and/or different ξ-parameter physics that drive different systems to different spin equilibria as in Eqs. (32) and (35).

2.4 Constraints on the stellar magnetic field

The basic assumptions underpinning the standard accretion model discussed in the preceding sections places some constraints on the stellar magnetic field.

The first constraint comes from the condition $R_{\rm A} > R_\star$ (i.e. the truncation of the disc takes place above the stellar surface) and leads to a lower limit for $B_\star$

$$B_\star > B_{\rm min} = \frac{\dot{M}^{1/2}(GM_\star)^{1/4}}{\xi^{7/4}R_\star^{5/4}}. \tag{36}$$

In a similar fashion, an upper limit for the magnetic field can be derived from the condition $x_{\rm A} < x_{\rm A,eq}$ (i.e. $N_{\rm tot} > 0$ during a spin-up episode),

$$B_\star < B_{\rm max} = \frac{x_{\rm A,eq}^{7/4}}{(2\pi)^{7/6}\xi^{7/4}}\frac{\dot{M}^{1/2}(GM_\star)^{5/6}}{\nu_\star^{7/6}R_\star^3}. \tag{37}$$

For a given $B_\star$ the above inequalities can be rearranged into constraints for ξ; these should be considered together with this parameter's previously discussed theoretical range (for example, in the $N_{\rm tot}^{\rm new(3)}$ torque model ξ should like below $\xi_{\rm max}$ for the system to be able to reach spin equilibrium). This issue is discussed further in a later section for specific cases of AMXPs.

Similar constraints can be derived for the magnetospheric radius $R_{\rm m}$ described by (20), although via a numerical solution.

2.5 Spin evolution

Given a total torque N, the (instantaneous) spin evolution of the system, $\dot{\nu}_\star$, is determined by balancing the shift in the rotational kinetic energy with that associated with N, i.e.,

$$\dot{\nu}_\star = \frac{N}{2\pi I_\star}, \tag{38}$$

where we have assumed that the moment of inertia is time independent, $\dot{I}_\star = 0$. Even during an active phase, the neutron star within the system will be subject to an electromagnetic braking torque, $N_{\rm EM}$, that acts to slow down the star. For a given accretion torque $N_{\rm acc}$ (i.e., one of those appearing in Tab. 1), the total torque acting on the star is thus $N = N_{\rm acc} - N_{\rm EM}$ (though see below).

During active phases where the source is especially bright, one expects that $N_{\rm acc} \gg N_{\rm EM}$, and so the braking term is ignored when modelling the spin evolution during an outburst. During a period of quiescence however, where negligible accretion torques are applied, the star will decelerate. We adopt the subscript 'Q' throughout to indicate quiescent phase predictions or measurements. By contrast, 'O' is similarly used to indicate an outburst phase.

Assuming pure (centred) dipole magnetic braking, the associated spin-down rate is given by a formula of the form

$$\dot{\nu}_{\rm Q} = -\frac{2\pi^2}{c^3}\frac{\mu_\star^2\nu_\star^3}{I_\star}K. \tag{39}$$

The parameter K encompasses different choices of spin-down model (we also note the factor 1/2 difference between our definition $\mu_\star = B_\star R_\star^3$ and that of the two papers cited below). The classic vacuum model (Gunn & Ostriker 1969) corresponds to $K = (1/3)\sin^2\vartheta$, where ϑ is the spin-magnetic axis misalignment angle. However, the standard practice of assuming a star that acts as an orthogonal rotator ($\vartheta = \pi/2$) does not sit well with the assumed axisymmetry of the accreting system. A more realistic approach would be to use the Spitkovsky (2006) formulae [see also Philippov, Spitkovsky & Cerutti (2015)], appropriate for an oblique rotator coupled to a force-free magnetosphere, as in Andersson, Jones & Ho (2014). This state-of-the-art model is described by $K \approx (1/2)(1+\sin^2\vartheta)$ and has the attractive property of predicting spin-down even for an aligned rotator.

We further note that expression (39) assumes negligible gravitational radiation and propeller torques. As such, the magnetic field estimates we obtain from spin-down should

[2] A rather different estimate for $R_{\rm m}$ comes from 3D MHD simulations of plasma flow (Kulkarni & Romanova 2013) in the form of a fitting formula $R_{\rm m} \approx (R_\star^3\mu_\star^4/\dot{M}^2GM_\star)^{1/10}$ that takes into account the non-dipolar deformation of the neutron star's magnetosphere.

Torque symbol	Functional form	Reference(s)
$N_{\rm A}$	$\dot{M}\sqrt{GM_\star R_{\rm A}}$	(Pringle & Rees 1972)
$N_{\rm m}$	$N_{\rm A}\,(1-\omega_{\rm A})$	[cf. Andersson et al. (2005)]
$N^{\rm W(2)}_{\rm tot}$	$\frac{1}{3}N_{\rm A}\,(7/2-4\omega)\,(1-\omega)^{-6/7}$	(Wang 1995)
$N^{\rm W(3)}_{\rm tot}$	$\frac{1}{3}N_{\rm A}\,\left(7/2-4\omega+\omega^2/3\right)(1-\omega)^{-6/7}$	(Wang 1995)
$N^{\rm R,BC}_{\rm tot}$	$\frac{2}{3}N_{\rm A}\left(2-\omega_{\rm A}+\frac{1}{3}\omega_{\rm A}^2\right)$	(Rappaport, Fregeau & Spruit 2004) (Bhattacharyya & Chakrabarty 2017)
$N^{\rm A}_{\rm tot}$	$\frac{1}{3}N_{\rm A}\left(7/2-7\omega+3\omega^2\right)(1-\omega)^{-6/7}$	(Andersson et al. 2005)
$N^{\rm new(3)}_{\rm tot}$	$\frac{2}{3}\xi^{-7/2}N_{\rm A}\left[\,\frac{1}{2}\left(1+3\xi^{7/2}\right)-\omega_{\rm A}+\frac{1}{3}\omega_{\rm A}^2\,\right]$	This paper
$N^{\rm new(2)}_{\rm tot}$	$\frac{1}{3}\xi^{-7/2}N_{\rm A}\left(1+3\xi^{7/2}-2\omega_{\rm A}\right)$	This paper

Table 1. A list of the accretion torques considered in this paper (see Section 2.2).

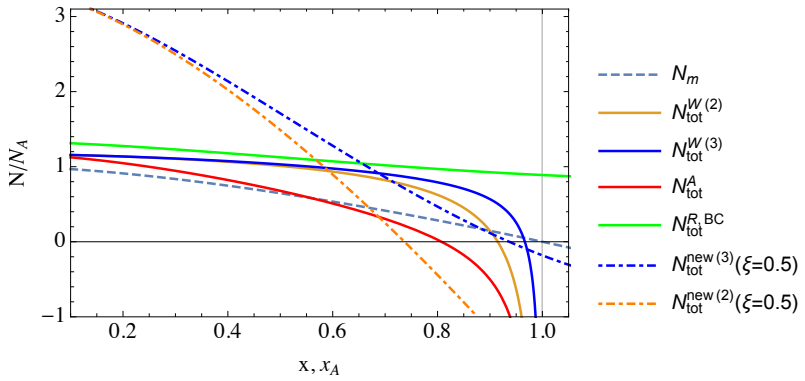


Figure 1. Comparison of the torques pigeonholed in Table 1 and discussed in Section 2.2. Each torque is normalised to the baseline torque $N_{\rm A}$ and is plotted as a function of the corresponding fastness parameter $x_{\rm A}$ or x. When plotting the two 'new' torques $N^{\rm new(2,3)}_{\rm tot}$ we factor out the ξ dependence of $N_{\rm A}$ and then evaluate the torque at the fiducial value $\xi=0.5$. $N=0$ marks the equilibrium x-point of each model (only the baseline torque $N_{\rm m}$ predicts $x_{\rm eq}=1$, see vertical line).

be treated as strict *upper limits* (the same estimates would instead represent lower limits if the quiescence phase were to include an unmodelled spin-up torque e.g. due to weak residual accretion). For example, should the star house a time-dependent mass quadrupole moment through the formation of an accretion-built mountain, radiation reaction will sap additional angular momentum from the system and a lower $B_\star$ would be required to accommodate a fixed $\dot{\nu}_{\rm Q}$ (Melatos & Payne 2005; Priymak, Melatos & Payne 2011). Numerical simulations of Ohmic (Vigelius & Melatos 2009) and thermal (Suvorov & Melatos 2019) relaxation suggest sufficiently light mountains can survive over long diffusion timescales ($\tau_{\rm diff}\gtrsim 10^5$ yr), and may therefore persist during quiescent phases if formed during a previous, active epoch [though cf. Mukherjee (2017)]. Because the GW torque scales sharply with the spin frequency, $N_{\rm GW}\propto\nu^5$, it has been suggested that bimodality in the distribution of spins in AMXPs, distinguishing the 'fast' and 'slow' populations, could be explained by the presence or absence of GW torques (Gittins & Andersson 2019). We will however assume that gravitational radiation is negligible for the remainder of this work, as these issues are beyond the scope of this paper [see, e.g., Patruno (2010) for a discussion].

3 CASE STUDIES: XTE J1751–305, IGR J00291+5934 & SAX J1808.4–3658

Using the torque models derived in the previous section, we are now in a position to compare theory with observation. Though we compile data relevant for several systems for completeness (see below), we focus primarily on three AMXPs in this paper: XTE J1751–305 (henceforth J1751), IGR J00291+5934 (J00291), and SAX J1808.4–3658 (J1808). Each of these sources have exhibited at least one well-timed outburst, where pulse timing revealed an increase in the respective spin frequencies between before and after phases. The first two of these were considered by Andersson, Jones & Ho (2014), who compared the baseline $N_{\rm A}$ and $N_{\rm m}$ torques against the observations, and by considering these systems in detail we can provide something of a one-to-one comparison with their results. In particular, as commented

by Andersson, Jones & Ho (2014), existing models of spin-up were unable to explain the measured $\dot{\nu}_{\rm O}$ values for these two objects during their respective 2002 and 2004 outbursts (see Fig. 2 therein). As will become clear, the discrepancy is even more extreme for J1808, which underwent a particularly violent episode of spin-up in 2015 (Sanna et al. 2017a). One goal of this work is to review the findings of Andersson, Jones & Ho (2014) using the various models presented in Tab. 1.

Table 2 lists data relevant for several AMXP systems. In particular, the second column gives the spin frequencies and the third lists the (mean) *spin-downs* measured during quiescence (though sometimes long-term averages are taken without excluding outburst rises), from which we estimate the polar field strength using expression (39) (third column). The final two columns list the mean *spin-up* and X-ray luminosities recorded during the relevant bursting episode, respectively. Some notes relevant to data for the individual systems listed in Tab. 2 and the general observational methodologies are given throughout the remainder of this section.

3.1 Observational and systematic uncertainties

The methods used to estimate changes in spin frequency, either during a bursting episode or in some quiescent epoch, vary in the literature. In the simplest timing method, one notes that the spin frequency changes by an amount $\Delta\nu$ during a time window of length τ, which implies a mean spin-up of $\Delta\nu/\tau$. Often, however, a more sophisticated timing model using Taylor expansions is employed; see, e.g., Papitto et al. (2008). Either way, typically only mean values for the spin-up and down can be reliably measured, and it is for this reason that averages are presented in Tab. 2 above. From a modelling perspective, one must effectively consider a time-averaged version of equation (38). Other complicated factors also play a role, such as the choice for the flux cutoffs where the burst is said to have concluded and handling correlations between the X-ray flux, pulse phases, and timing noise; compare, for instance, the spin-ups reported for the 2004 outburst of J00291 between Falanga et al. (2005) [$\langle\dot{\nu}_{\rm O}\rangle = 8.4(6)\times10^{-13}$ Hz s^{-1}] and Patruno (2010) [$\langle\dot{\nu}_{\rm O}\rangle = 5.1(3)\times10^{-13}$ Hz s^{-1}]. Reported spin-downs are also average values obtained from timing over long observational windows, usually several years; compare the quiescent spin-downs reported for J00291 between Patruno (2010) [$\langle\dot{\nu}_{\rm Q}\rangle = -3.0(8)\times10^{-15}$ Hz s^{-1}] and later by Papitto et al. (2011) [$\langle\dot{\nu}_{\rm Q}\rangle = -4.1(12)\times10^{-15}$ Hz s^{-1}]. For concreteness, the latter results are employed in this work. In some cases (most notably J1808) different estimates for the spin-down immediately following outbursts are recorded; see Sec. 3.4.

From a calibration perspective, accurately determining the peak (and mean) X-ray luminosities for the objects listed here requires one to 'correct' the raw flux data. Radiation is scattered and absorbed by the interstellar medium en route to the detector(s), resulting in the instrument reporting a lower flux than is truly being emitted, the extent of which depends on the (spatially-varying) hydrogen column density; see Lattimer & Steiner (2014) for a detailed discussion. Furthermore, X-ray burst emissions are generally composed of thermal components, originating from the stellar surface and possibly the disc, and a scattered Compton component, originating from some height above the surface (e.g., Keek et al. 2018). Models aiming to account for these effects differ slightly in the literature (see, e.g., the Comptonization model of Gierliński & Poutanen 2005), resulting in different (post-processed) light curves. Finally, determining the mean luminosity from a given light curve can itself be subject to model variability. In many cases, the flux observed from bursts tends to show an exponential decay, and therefore one can — assuming that the X-ray flux is a good tracer of $\dot{M}$ — write the mass accretion rate during a burst as $\dot{M}(t) \sim \dot{M}_{\rm peak}\exp\left[(t-T_0)/\tau\right]$ (Burderi et al. 2006), where τ is the characteristic e-folding decay time and T_0 is some reference time. From this expression one finds the mean, $\langle\dot{M}\rangle \sim 0.63\dot{M}_{\rm peak}$.

Assumptions on the efficiency of the system can also play a role, as there is some energy lost in converting between the 'accretion' and X-ray luminosities. Generally, a factor of $\sim$ 1–2 is accounted for in this respect, but different authors consider different factors. Furthermore, assumptions on the distance and whether the source is radiating isotropically or narrowly beaming both affect the estimate for the true, bolometric luminosity [see equation (9) in Ng et al. (2021)]. Finally, it is important to note that magnetic field and torque estimates scale with the stellar mass and radius in various ways. For instance, in expression (39) one sees that $B_\star \propto M_\star^{1/2}R_\star^{-2}$ for fixed $\dot{\nu}_{\rm Q}$. While it is traditional to take the canonical values $M_\star = 1.4M_\odot$ and $R_\star = 10$ km, these may not be appropriate for all LMXB systems[3]. For instance, using the 1998 outburst data for J1808, Li et al. (1999) found that the neutron star may be very compact; for $R_\star = 10$ km, the *minimum* mass they estimate is $M_\star \approx 2M_\odot$. Since $L_{\rm X} \sim GM_\star\dot{M}/R_\star$, taking instead a value $M_\star = 2M_\odot$ leads to a $\lesssim 40\%$ *decrease* in the inferred accretion rate $\dot{M}$, which is the relevant quantity appearing within the baseline torque $N_{\rm A}$. We additionally assume throughout that $I_\star \approx 0.38M_\star R_\star^2$, in accord with the GR calculation for a Tolman-VII equation of state with a star of canonical compactness (Lattimer & Prakash 2001).

3.2 XTE J1751–305

Table 2 reports data relevant for the 2002 outburst of J1751. Before presenting a detailed comparison between torque models, we note that the peak luminosity given by Riggio et al. (2011) [$L_{\rm max,36} \sim 11.6\,d_{8.5}^2$; the value used by Andersson, Jones & Ho (2014)] is smaller than that of Gierliński & Poutanen (2005) ($L_{\rm max,36} \sim 27\,d_{8.5}^2$) [see also Papitto et al. (2008)]. These latter references include a Comptonization component, which suggests the true (bolometric) luminosities are roughly twice as large as the raw values, which is likely the cause of the discrepancy. The distance to this object is thought to be between 6.7 and 9.1 kpc (Papitto et al. 2008), which could lead to a factor $\sim$ 2 adjustment in the calculated X-ray luminosity in either case.

[3] According to the latest results from the Neutron Star Interior Composition Explorer (NICER), a more realistic radius for a star with a canonical mass $M_\star = 1.4M_\odot$ is $R_\star \approx 12$ km (Miller et al. 2021). A $\sim 20\%$ increase in $R_\star$ can have a non-negligible effect in expressions that scale strongly with radius, such as (39).

Table 2. Observed and derived properties related to the five AMXPs considered in this work. The polar field strength, $B_\star$, is derived from the given (mean) quiescent spin-down rate $\langle\dot{\nu}_{\rm Q}\rangle$ through the braking formula (39) with $K=(1+\sin^2\vartheta)/2$, where the given uncertainties incorporate the range $0\leqslant\vartheta\leqslant\pi/2$. The magnetic field estimate is made assuming $M_\star=1.4M_\odot$ and $R_\star=10$ km, where we use the Tolman-VII moment of inertia, $I_\star\approx 0.38M_\star R_\star^2$. X-ray luminosities are computed from 'corrected' fluxes (see text), where the assumed distance is given explicitly through the subscripts (e.g., $d_{8.5}$ indicates that a distance of $d=8.5$ kpc was assumed to convert between fluxes and luminosities). See text for comments on individual source data.

Source	$\nu_{\rm spin}$ (Hz)	$\langle\dot{\nu}_Q\rangle$ (Hz s^{-1})	$B_\star(\times10^8$ G)	$\langle\dot{\nu}_O\rangle$ (Hz s^{-1})	$\langle L_{\rm X}\rangle$ ($\times10^{36}$ erg s^{-1})
XTE J1751–305 (2002)[a]	435.3	$-5.5(12)\times10^{-15}$	3.8(10)	$3.7(10)\times10^{-13}$	$\sim 17\times d_{8.5}^2$
IGR J00291+5934 (2004)[b]	598.9	$-4.1(12)\times10^{-15}$	2.0(7)	$5.1(3)\times10^{-13}$	$\sim 2.7\times d_{4.2}^2$
2015 Outburst[c]				$3(5)\times10^{-12}$	$\lesssim 0.72\times d_{4.2}^2$
SAX J1808.4–3658 (1998)[d]	401.0	$-5.5(12)\times10^{-16}$	1.3(4)	$<2.5\times10^{-14}$	$\lesssim 5.1\times d_{3.5}^2$
2002 Outburst[e]		$-7.6(15)\times10^{-14}$	16(4)	$4.4(8)\times10^{-13}$	$\sim 6.3\times d_{3.5}^2$
2015 Outburst[f]		$-1.5(2)\times10^{-15}$	2.2(5)	$2.6(3)\times10^{-11}$	$\lesssim 2.6\times d_{3.5}^2$
XTE J1814–338 (2003)[g]	314.4	$\sim -8.7(4.2)\times10^{-15}$	$\sim 8.2(32)$	$<1.5\times10^{-14}$	$\lesssim 2.2\times d_8^2$
IGR J17494–3030 (2020)[h]	376.1	$-2.1(7)\times10^{-14}$	9.2(30)	$<1.8\times10^{-12}$	$\gtrsim 1.1\times d_{10}^2$

References: [a] Gierliński & Poutanen (2005); Papitto et al. (2008); Riggio et al. (2011). [b] Falanga et al. (2005); Patruno (2010); Papitto et al. (2011). [c] Tudor et al. (2017); Sanna et al. (2017b) [though cf. De Falco et al. (2017)]. [d] Hartman et al. (2009); Haskell & Patruno (2011). [e] Burderi et al. (2006) [though cf. Chakrabarty et al. (2003)]. [f] Sanna et al. (2017a); Tudor et al. (2017). [g] Krauss et al. (2005); Haskell & Patruno (2011); Baglio et al. (2013). [h] Ng et al. (2021).

Figure 2 compares the theoretical spin-up of J1751 during the 2002 outburst for the Rappaport, Fregeau & Spruit (2004) and Bhattacharyya & Chakrabarty (2017) model $N_{\rm tot}^{\rm R,BC}$ (dotted curve) with the new models $N_{\rm tot}^{\rm new(2)}$ (red) and $N_{\rm tot}^{\rm new(3)}$ (orange) considered here. In particular, since the former torque is the largest of all others [with the exception of new(2,3)] for the whole range of $x_{\rm A}$ (see Fig. 1), it represents a maximum amongst the 'classical' models.

We see that the spin-up using $N_{\rm tot}^{\rm R,BC}$ is only marginally consistent with the observations: for the maximum predicted values of $B_\star$ from spin-down (see Tab. 2), the theoretical torque just scrapes the lower-limit of $\langle\dot{\nu}_{\rm O}\rangle$. Since this torque is larger than the baseline models $N_{\rm A}$ and $N_{\rm m}$, our finding is consistent with those of Andersson, Jones & Ho (2014), since in this case the theoretical maxima would lie below the observed minimum. The situation is worse if one instead uses the smaller of the two X-ray luminosities discussed above, as was done by Andersson, Jones & Ho (2014). However, we see that both $N_{\rm tot}^{\rm new(2,3)}$ can comfortably accommodate even the maximum values of spin-up for $\xi=0.45$ for the measured range of $B_\star$. Since values $\xi<1$ are consistent with the prediction (5) for canonical values of disc thickness and viscosity, we conclude that the simple, analytic models considered here are consistent with the observations for this object. Note that the equilibrium values of the fastness parameter differ between models (2) and (3), and $N_{\rm tot}^{\rm new(2)}$ falls to zero at a lower $B_\star$ value than its slightly larger counterpart for $\xi=0.45$ [see Eqs. (32) and (35)]. Either way, we have that $B_{\rm max}$ exceeds the maximum allowed by spin-down.

Although we take a fixed value of $\xi=0.45$ above, there typically is, for a given torque model and $B_\star$, a range of ξ such that the predicted spin-up lies within a desired band. In Figure 3 we show (blue curves) the theoretical $\xi-B_\star$ parameter space, associated with $N_{\rm tot}^{\rm new(3)}$, such that $2.7\leqslant\dot{\nu}/(10^{-13}\ {\rm Hz\ s^{-1}})\leqslant 4.7$ (see Tab. 2). The grey region instead shows the range of $B_\star$ and ξ such that inequalities (36) and (37), set by the geometric requirements of the disc, are satisfied. In particular, if ξ is too large for some fixed $B_\star$ then the model does not permit an equilibrium fastness parameter [see also Eq. (30)], while if ξ is too small for some fixed $B_\star$ then the Alfvén radius will cut into with the star. The final region of interest in Fig. 3 is the magenta column which shows, as in Fig. 2, the $B_\star$ range predicted by spin-down. The complicated shape that is formed by the intersection of all three surfaces described above yields the theoretically- and observationally-allowed parameter space for this object. Note, however, that this range is itself sensitive to the other (uncertain) parameters intrinsic to the system (e.g., $M_\star$, $R_\star$, $\dot{M}$, ...).

3.3 IGR J00291+5934

Table 2 reports data relevant for the 2004 and 2015 outbursts of J00291, which are discussed in detail below. Some notes are as follows. Assuming the 2015 burst was of a pure helium nature, De Falco et al. (2017) constrained the distance of J00291 to be 4.2 ± 0.5 kpc. Falanga et al. (2005) report a *peak* luminosity of 6.3×10^{36} erg s^{-1}, though assumed $d=5$ kpc [see also Andersson, Jones & Ho (2014)]. The luminosity for the 2015 outburst is inferred from data given in Tudor et al. (2017), who did not include comptonization or bolometric corrections, by adopting the correction factor used by Falanga et al. (2005) for the 2004 burst. Note however that the peak and mean values for both the 2004 and 2015 bursts differ between De Falco et al. (2017) and Falanga et al. (2005); Tudor et al. (2017), respectively: the former authors suggest a higher ($\sim 40\%$) flux (see Table 2 therein).

Similar to Fig. 2, Figure 4 compares theory with observation for the 2004 outburst of J00291. In this instance, again noting that $N_{\rm tot}^{\rm R,BC}$ is the largest amongst the 'classical' models, we see that the various (analytic) torque expressions thus far considered in the literature are utterly unable to accommodate the spin-up for this object, as concluded by

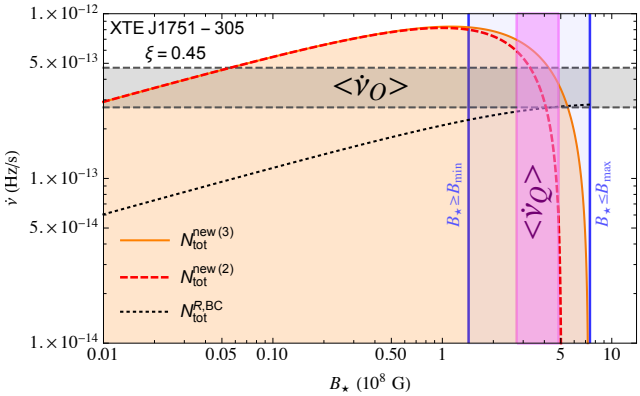


Figure 2. A comparison between predicted spin-evolutions [via Eq. (38)] for $N_{\rm tot}^{\rm R,BC}$ (dotted black curve), $N_{\rm tot}^{\rm new(2)}$ (dashed red curve), and $N_{\rm tot}^{\rm new(3)}$ (orange curve), as functions of $B_\star$, for the 2002 outburst of J1751. The measured spin-up is shown in the grey band, while the blue lines to the left and right illustrate the minimum and maximum magnetic field strengths [for new(3)] permitted through the requirements $R_{\rm A} > R_\star$ and $R_{\rm A} < x_{\rm A,eq}R_{\rm co}$, respectively; see Eqs. (36)-(37). The region bounded by the magenta column represents the *total* uncertainty in the magnetic field strength, as calculated by combining the observational uncertainty in the mean spin-down $\langle\nu_{\rm Q}\rangle$ and the variation $0 \leqslant \vartheta \leqslant \pi/2$ in the magnetic axis inclination. A fixed value of $\xi = 0.45$ is taken.

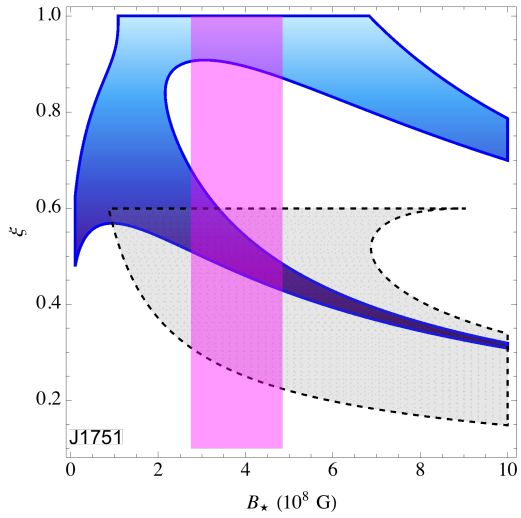


Figure 3. The allowed $\xi - B_\star$ parameter space for the 2002 outburst of J1751. The blue region shows the theoretical combinations of ξ and $B_\star$ for which $\dot\nu$, from $N_{\rm tot}^{\rm new(3)}$, takes a value within the range set by the outburst data. The magenta column shows the predicted range of $B_\star$ from quiescent spin-down, while the grey surface delimits the space over which ξ and $B_\star$ respect the geometric requirements of the disc. The intersection between all three regions gives the range of ξ and $B_\star$ consistent with observation for the torque model $N_{\rm tot}^{\rm new(3)}$.

Andersson, Jones & Ho (2014). In particular, even for extreme values of $B_\star \lesssim 5 \times 10^8$ G – the maximum allowed by the requirement that $R_{\rm A} < x_{\rm A,eq}R_{\rm co}$ – the largest value of $\dot\nu$ from $N_{\rm tot}^{\rm R,BC}$ is an order of magnitude below the reported value $\langle\dot\nu_{\rm O}\rangle$. Furthermore, tweaking the mass, radius, or moment of inertia of the star within reasonable ranges is not able to alleviate the discrepancy. By contrast, for the model $N_{\rm tot}^{\rm new(3)}$ with $\xi = 0.27$, we see that the whole range of the observed spin-up can be met. Similar conclusions are found for $N_{\rm tot}^{\rm new(2)}$.

In 2015 the object went into outburst again, though this time displayed a $\gtrsim 6$ times higher degree of spin-up than in 2004 (Sanna et al. 2017b), even though the X-ray luminosity was smaller by a factor $\lesssim 4$ [see Tab. 1; though cf. De Falco et al. (2017)]. As such, unless we seriously underestimate the accretion rate $\dot M$ (cf. Sec. 4.3), the 'classical' models fall very short (by ~ 2 orders of magnitude) of being able to explain the spin-up in this case. If instead we take a value $\xi = 0.11$ and a slightly more compact star than in Fig. 4 with $GM_\star/c^2R_\star \sim 0.24$ however, even the extreme, upper-limit value of $\langle\dot\nu_{\rm O}\rangle$ can be matched using the torque $N_{\rm tot}^{\rm new(3)}$, as shown in Fig. 5. This matching however requires the magnetic field to be on the low end within the allowed region, i.e., that $R_{\rm A} \sim R_\star$. GR effects, which we have thus far ignored, may therefore be important since the spacetime is expected to be strongly non-Minkowski near the stellar surface (see Sec. 4.2).

Similar to Fig. 3, Figure 6 shows allowed combinations of ξ and $B_\star$ for the 2004 (left panel) and 2015 (right panel) outbursts of J00291. The blue strips show the theoretical values of $\dot\nu$, again calculated from $N_{\rm tot}^{\rm new(3)}$, consistent with the observed spin-ups, while the grey region delimits the geometrically-set ranges of ξ and $B_\star$. Note also that since we take slightly different compactness values between Figs. 4

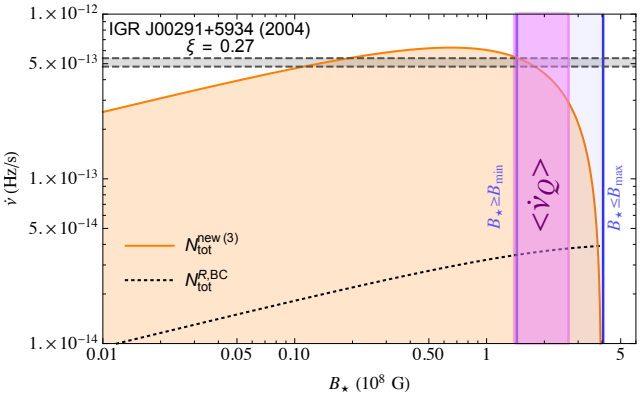


Figure 4. Similar to Fig. 2 but for the 2004 outburst of J00291. A fixed value of $\xi = 0.27$ is taken.

and 5 for demonstration purposes, the observational range of $B_\star$ [Eq. (39)] and the theoretical range of ξ and $B_\star$ [Eqs. (36) and (37)] differs between the two cases. We see that in either case the constraints on ξ and $B_\star$ are stricter than for J1751; for the 2004 data this is because the error bars on $\langle\dot\nu_O\rangle$ are much tighter, while in 2015 the spin-up was so extreme that it is difficult to produce the required torque unless ξ is taken close to the theoretical minimum where $R_A \gtrsim R_\star$, as described above. Physically speaking, these findings suggest that the disc in this system may be less viscous and/or thinner than for J1751, and that α, H, or $R_{\rm A}$ are dynamical over $\sim$ year-long timescales; see expression (5).

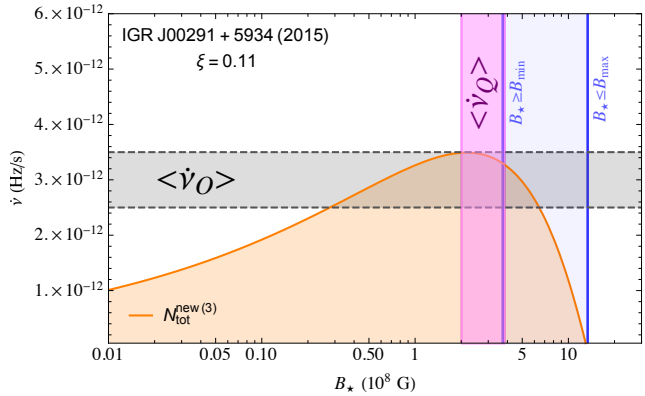


Figure 5. Theoretical spin-up predicted using $N_{\rm tot}^{\rm new(3)}$ (orange curve), as a function of $B_\star$, for the 2015 outburst of J00291. Other torque models are not shown, since they lie well-below the y-axis range shown here. A fixed value of $\xi = 0.11$ is taken.

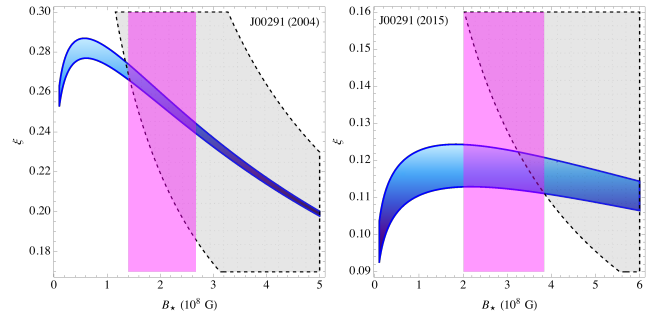


Figure 6. Similar to Fig. 3, though for the 2004 (left panel) and 2015 (right panel) outbursts of J00291. Note that slightly different compactness values are taken between the two cases for demonstration purposes, so that the spin-down constraints on $B_\star$ (magenta columns) differ slightly.

3.4 SAX J1808.4–3658

Finally, we also consider the system J1808, which was not studied by Andersson, Jones & Ho (2014). Some relevant notes are as follows. The quiescent spin-down rate from Hartman et al. (2009) [$\langle\dot{\nu}_{\rm Q}\rangle = -5.5(12)\times10^{-16}$ Hz s^{-1}] differs from Sanna et al. (2017a) [$\langle\dot{\nu}_{\rm Q}\rangle = -1.5(2)\times10^{-15}$ Hz s^{-1}], possibly because spin-down was accelerated during those 8 years or because spin-up during outburst episodes were handelled in a statistically different way [see Sanna et al. (2017a) for a discussion]. More extremely, for the 2002 burst data specifically, Burderi et al. (2006) report a value of $\langle\dot{\nu}_{\rm Q}\rangle = -7.6(15)\times10^{-14}$ Hz s^{-1} for the spin-down. Using the traditional braking formula (39) thus implies a factor ~ 10 larger dipole moment relative to the other epochs, because of the factor ~ 100 increase in the magnitude of $\dot{\nu}_{\rm Q}$ (see fourth column of Tab. 2). Burderi et al. (2006) suggest that a smaller value of $B_\star \lesssim 4\times10^8$ G is obtained if one instead assumes that the spin-down torque is due to the magnetic drag on the accretion disc [specifically, they apply Eq. (23) of Rappaport, Fregeau & Spruit (2004)]. Taken literally in the context of expression (39) however, these timing fits suggest that the spin-down of the object varies substantially on timescales of ~ 10 yr, possibly indicating rapid magnetic field evolution or the formation of an accretion-built mountain. We note that distance measurements for this object are rather tight, viz. $d = 3.5(1)$ kpc (Galloway & Cumming 2006), so much larger values of $L_{\rm X}$ are unlikely. Data for the 2015 outburst come from the XMM Newton measurements rather than those from NuSTAR, the latter of which predicts an even more extreme spin-up (by a factor ~ 10). Sanna et al. (2017a) suggest that the NuSTAR measurements are overly large because of the time drift within the internal clock of the instrument.

Figure 7 compares the theoretical spin-up predicted by $N_{\rm tot}^{\rm new(3)}$ for the 2015 outburst of J1808. In particular, the spin-up achieved during this period, according to Sanna et al. (2017a), is the most extreme of all systems thus far observed. The X-ray luminosity found during the outburst was not particularly high however, and so, much like in the case of J00291, the 'classical' models are not able to come close to explaining the spin-up here (though they can for the 1998 and 2002 outbursts). In fact, the spin-up is so large that even the model $N_{\rm tot}^{\rm new(3)}$ cannot account for the data unless we use the spin-down estimates for the 2002 burst (Burderi et al. 2006) and take $\xi \lesssim 0.1$. In particular, using the spin-down values $\langle\dot{\nu}_{\rm Q}\rangle$ for either the 1998 and 2015 cases returns $B_\star$ values which are much smaller than the requirement set by $R_{\rm A} > R_\star$, see Eq. (36).

It is interesting to note however that in 2008, XMM-Newton and Suzaku captured a relativistically-broadened K-α iron line at ~ 6.5 keV in the spectrum of J1808 (Papitto et al. 2009; Cackett et al. 2009). It is generally thought that these emission lines originate from the inner edge of the accretion disc, and therefore their spectra can, in principle, be used to determine the magnetospheric radius (Patruno & Watts 2021). For J1808, the emission spectra suggest this radius lies at $\sim 4.4^{+1.8}_{-1.4}$ Schwarzschild radii (Papitto et al. 2009). For a star with $M = 2.0M_\odot$, as found by Li et al. (1999), we therefore obtain $B_\star \gtrsim 2(\xi/0.1)^{-7/4}\times10^9$ G by matching expression (4) with the above, which agrees with the value inferred from spin-down measured in 2002 and the values needed to explain the 2015 outburst.

Regardless, there appears to be some conflict between the ranges of $B_\star$ inferred from different epochs. We are therefore left with a few possible conclusions. (i) The reported spin-up in 2015 is an overestimate, possibly for the reasons described in Sec. 3.1 or in Sanna et al. (2017a). (ii) The reported spin-down (for the 2015 burst) is too low, or (iii) there is some physics that becomes important for extreme values of $\xi \lesssim 0.1$ that is not included in the description of the torque models. To conclusively rule out option (iii) one requires 3D simulations of realistic matter flows in accreting neutron stars, such as those described in Kulkarni & Romanova (2013). In any case, the message here is that there are still several unanswered questions concerning spin evolution in AMXPs.

4 ADDITIONAL PHYSICS TO CONSIDER

Accreting neutron stars are almost by default rather 'dirty' physical systems and as a consequence the magnetospheric accretion model described in Section 2.2 is unlikely to capture all of the relevant physics. In this section we discuss in more detail some of the most important corrections to that model, namely, the likely multipolar structure of the

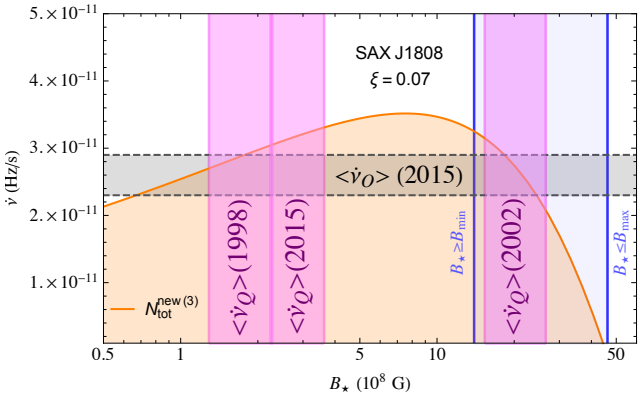


Figure 7. Theoretical spin-up predicted using $N_{\rm tot}^{\rm new(3)}$ (orange curve), as a function of $B_\star$, for the 2015 outburst of J1808. For this object we take a compact star with $M_\star = 2.0 M_\odot$ and $R_\star = 10$ km, in line with the findings of Li et al. (1999). Other torque models are not shown, since they lie well-below the y-axis range shown here. We show the predicted $B_\star$ values from spin-downs reported by different authors for separate epochs in the various magenta columns (see Tab. 2). A fixed value of $\xi = 0.07$ is taken.

magnetic field and the impact of GR gravity. It should be pointed out that none of these effects change the main conclusions of this paper but could help alleviate the tension seen in some systems as in, for example, J00291's spin-up during its 2015 outburst (see Fig. 5).

4.1 Multipolar magnetic fields

Assuming a force-free magnetosphere[4] the poloidal field can be expressed as a sum of force-free multipoles. In most models considered in the literature, only the dipole component is kept for simplicity, as in Sec. 2. However, recent observations of hot spot activity on PSR J0030+0451 (Bilous et al. 2019) and GRO J1744–28 (Doroshenko et al. 2020), together with cyclotron resonant scattering features seen in several accretion-powered X-ray pulsars (Staubert et al. 2019), suggest that the magnetic fields of stars with a history of accretion are likely to contain non-negligible multipole components near the stellar surface. Theoretical considerations support this conclusion, as comparable multipole moments are seen to form from seeding dipole fields in simulations of crustal Hall drift coupled with (accretion-accelerated) Ohmic decay (Urpin & Geppert 1995; Rheinhardt & Geppert 2002; Cumming, Arras & Zweibel 2004) and accretion-induced magnetic burial (Priymak, Melatos & Payne 2011; Suvorov & Melatos 2020). Nevertheless, since a general ℓ-pole falls off like $r^{-(2+1)\ell}$, the dipole component will typically dominate at large radii ($r \gg R_\star$). Unless the field is sufficiently weak therefore such that the Alfvén radius lies close to the stellar surface, one can typically ignore higher-multipoles for the purpose of accretion torque modelling. For completeness however, we consider here a field with a strong quadrupole to illustrate the impact of multipolar components on the behaviour of the accretion torque.

This is achieved by introducing a dimensionless parameter κ, which quantifies the strength of the quadrupole field, through

$$B_z = -\frac{B_\star R_\star^3}{r^3}\left(1 + \kappa \frac{R_\star^2}{r^2}\right). \tag{40}$$

Non-dipolar terms directly influence the Alfvén radius, as the roots of the Euler equation (1) are necessarily shifted (see also Sec. 4.1). For magnetic fields consisting of mixed multipoles, finding these roots generally requires numerical methods. The functional forms for the accretion torques, given as integrals over some weighted magnetic energy density, are also adjusted. For instance, in the spirit of 'mechanism (3)' described by Wang (1995), we find, from Eq. (15),

$$\begin{aligned} N_{\rm disc} &= -\int_{R_{\rm A}}^{\infty} dr r^2 f_{(3)}(r) B_z(r)^2 \\ &= N_{\rm dip}\left[1 + \frac{18\kappa}{455}\left(\frac{R_\star}{R_{\rm A}}\right)^2 \left(\frac{91 - 130\omega_{\rm A} + 18\omega_{\rm A}^{10/3}}{3 + 2\omega_{\rm A}^2 - 6\omega_{\rm A}}\right)\right. \\ &\quad \left. + \frac{9\kappa^2}{1309}\left(\frac{R_\star}{R_{\rm A}}\right)^4 \left(\frac{187 - 238\omega_{\rm A} + 18\omega_{\rm A}^{14/3}}{3 + 2\omega_{\rm A}^2 - 6\omega_{\rm A}}\right)\right]. \end{aligned} \tag{41}$$

Using expression (41), we compare the total torques, $N_{\rm A} + N_{\rm disc}$, obtained for pure dipole ($\kappa = 0$) and strong quadrupole ($\kappa = 4$) cases, for parameters relevant to J1751, in Fig. 8. Including a quadrupole component tends to flatten the torque curve, i.e., $N_{\rm tot}^{\rm new(3)}$ varies slower as a function of $B_\star$ for greater κ. For fixed values of ξ, we see that the maximum torque that can be achieved is lower in the quadrupole case (by a factor ~ 2 for $\kappa \sim 4$) though, for $\xi = 0.45$, the mixed case is still able to accommodate the upper limits set by Papitto et al. (2008) for J1751's spin-up. We see also that $N_{\rm m}$, shown by the dotted curve, lies well below the spin-up band with or without quadrupole fields. Including a quadrupole component shifts the minimum and maximum values of the B field (as detailed in Sec. 2.4), as set by the geometrical requirements of the magnetosphere, to the left. Specifically, since the quadrupole is strong at the stellar surface, the spin-down and minimum are shifted more noticeably than the maximum, which is set by the physics occurring near the co-rotation radius. Note in particular that the electromagnetically-induced spin-down for a mixed dipole-quadrupole field reads (Pétri 2019)

$$\dot{\nu}_{\rm Q} = -\frac{2\pi^2 \mu_\star^2 \nu_\star^3}{3 I_\star c^3}(1+\kappa)\left[1 + \frac{64\pi^2}{45}\kappa^2\left(\frac{R_\star \nu_\star}{c}\right)^2\right], \tag{42}$$

where in the absence of a Spitkovksy-like formula for the field considered here we have assumed the standard model of an orthogonal rotator in vacuum (i.e., $K = 1/3$). This expression implies that the inferred $B_\star$ is also sensitive to κ, as can be seen from the magenta bars in Fig. 8.

4.2 General-relativistic corrections

Throughout our analysis thus far, we have restricted our attention to Newtonian equations of motion. There are, how-

[4] Though such a description may not be valid in the accretion layer near the stellar surface, where diamagnetic screening currents reside (Choudhuri & Konar 2002), it is likely a fair description at the Alfvén radius (see, e.g., the Grad-Shafranov simulations of Wette, Vigelius & Melatos 2010; Suvorov & Melatos 2020).

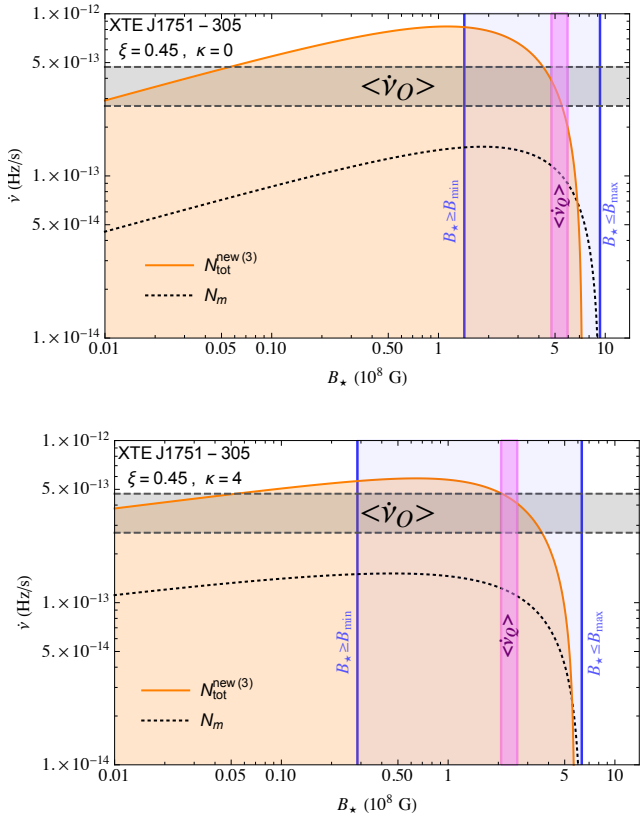


Figure 8. Baseline magnetospheric (black, dotted) and new(3) (orange, solid) accretion torques, as functions of the characteristic magnetic field strength $B_\star$, for J1751. The top panel shows the pure dipole case ($\kappa = 0$), while the bottom panel illustrates a case with a strong quadrupole component, $\kappa = 4$ [see Eq. (40)]. Each torque assumes canonical stellar parameters, $\xi = 0.45$, and the spin-down formula (42) to determine the range of $B_\star$ values that agree with the quiescent measurement $\langle \dot{\nu}_{\rm Q} \rangle$. Note that $B_{\rm max}$ corresponds to the torque $N_{\rm m}$.

ever, a number of places where GR corrections are likely to play a role, especially for very compact stars [such as J1808 (Li et al. 1999)]. In GR, the Euler and induction equations [Eqs. (1) and (13)] become weighted by the spacetime metric coefficients, most notably by the 'tt' Schwarzschild redshift factor, $z \sim 1 - 2GM_\star/c^2R_\star$. For rapidly rotating stars [such as J00291], rotational corrections to the geometry, including precession (see Sec. 4.3), may also become important as Birkhoff's theorem can no longer be faithfully applied to describe the spacetime exterior to the star (see, e.g., Pappas & Apostolatos 2012). These factors will shift the geometric radii important to the accretion problem, such as $R_{\rm A}$ and $R_{\rm co}$. Ultimately however, many of these corrections can be absorbed by our phenomenological parameters, such as ξ [i.e., by making the replacement $\xi_{\rm GR} \approx z^{-1}\xi_{\rm N}$], which depend sensitively on the flow particulars and are highly uncertain. Including relativistic corrections self-consistently requires one to solve the full GR-MHD system of equations, which is beyond the scope of this work [cf. Kulkarni & Romanova (2013)].

One can however get a clean but rough estimate for the importance of GR corrections by considering Post-Newtonian (PN) expansions. That is, by expanding the Einstein equations in powers of c^{-2}. As shown by Blanchet, Faye & Ponsot (1998), the Keplerian velocity profile at 2PN reads

$$\Omega_{\rm K}^{\rm 2PN}(r) = \Omega_{\rm K}(r)\left(1 - 3\mathcal{C}\frac{R_\star}{r} + 6\mathcal{C}^2\frac{R_\star^2}{r^2}\right)^{1/2}, \qquad (43)$$

where

$$\mathcal{C} = \frac{GM_\star}{c^2 R_\star}, \qquad (44)$$

is the stellar compactness. Though somewhat tedious, one could simply repeat the calculations performed in Sec. 2 using the rotational profile (43) instead of the standard Keplerian one, $\Omega_{\rm K}$. Consider just Eq. (1), which implies that the Alfvén radius resides at the solution to

$$\dot{M}\frac{d}{dr}\left[\Omega_{\rm K}^{\rm 2PN}(r)r^2\right]_{R_{\rm A}} = -R_{\rm A}^2\left(B_\phi B_z\right)_{R_{\rm A}}. \qquad (45)$$

Even for a dipolar magnetic field, the roots of expression (45) must be found numerically because of the high-order nature of the polynomial involved. Similarly, the corotation radius, defined as the point where $\Omega_{\rm K}^{\rm 2PN}(R_{\rm co}) = 2\pi\nu_\star$, must also be evaluated numerically.

Figure 9 shows two different Alfvén radii at 2PN order as functions of the magnetic field strength $B_\star$ for J1751. In particular, we consider the case of a less compact star with $\mathcal{C} = 0.2$ (black curve) and a more compact one with $\mathcal{C} = 0.3$ (red curve). As expected, the deviation, relative to the Newtonian approximation (4), is larger for the more compact case ($\sim 20\%$ larger at $B_\star = 10^8$ G). As the magnetic field strength increases, the Alfvén radius moves further away from the stellar surface, and the PN terms become less important. As such, in both examples with $\xi = 0.5$ (ignoring the distinction between $\xi_{\rm N}$ and $\xi_{\rm GR}$), the corrections become negligible for $B_\star \gtrsim 3\times10^8$ G where $R_{\rm A} \gtrsim 2R_\star$. Note, however, that for smaller values of ξ or larger values of $\mathcal{C}$, the Alfvén radius moves closer to the surface of the star [as can be seen from expression (4)] and the PN terms remain important for a wider range of $B_\star$. For J1751, where a value $B_\star \approx 5.3\times10^8$ G is predicted from spin-down (Riggio et al. 2011), we conclude that PN corrections are likely to be negligible. However, since $\nu_\star = 435$ Hz for this object, we can also calculate that the corotation radius is shifted by a factor $R_{\rm co}^{\rm 2PN}/R_{\rm co} \approx 0.92$ for a compactness $\mathcal{C} = 0.25$. Since this ratio is smaller than one, this implies that the fastness parameter $\omega_{\rm A}$ is larger than its Newtonian counterpart (by $\sim 10\%$), which leads to a marginally smaller torque in most models (cf. Fig. 1).

4.3 Disc tearing via Lense-Thirring precession

For a rotating source, Lense-Thirring (LT) precession appears as soon as we move from Newtonian to GR gravity. This key effect should be present when the disc is locally misaligned with the stellar spin axis, in other words when the disc is locally non-equatorial (Bardeen & Petterson 1975). LT dynamics have been extensively studied in accreting black holes; detailed calculations suggest that it may cause the disc to fragment in a series of precessing rings (Nixon et al. 2012; Raj & Nixon 2021). In this section we retrace the calculation of Nixon et al. (2012), although having LMXBs in mind instead of black holes.

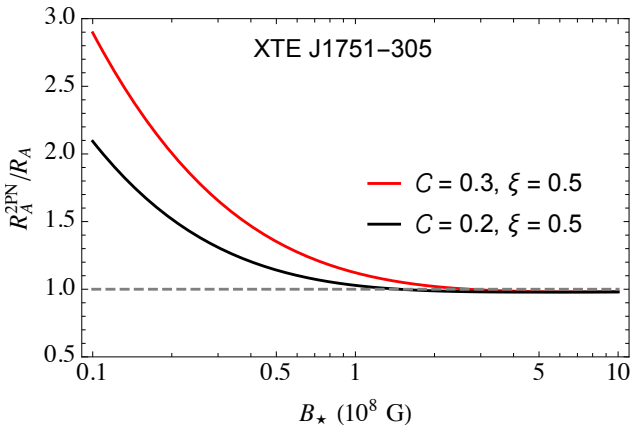


Figure 9. Normalised 2PN Alfvén radii as functions of $B_\star$ for stars with compactness $\mathcal{C} = 0.2$ (black curve) and $\mathcal{C} = 0.3$ (red curve). A value of $\xi = 0.5$ is chosen, though smaller (larger) values lead to a greater (lesser) shift relative to the Newtonian value, $R_{\rm A}$. We take an accretion rate $\dot{M} \sim 10^{-9} M_\odot$/yr, as appropriate for J1751 (see Tab. 2).

To leading PN order, the stellar spin-driven LT torque on the disc is given by the formula,

$$N_{\rm LT} = 2\pi r H |\mathbf{\Omega}_{\rm LT} \times \mathbf{L}|, \tag{46}$$

where

$$\mathbf{\Omega}_{\rm LT}(r) = \frac{2G}{c^2 r^3}\mathbf{J}_\star, \tag{47}$$

is the vectorial LT angular precession frequency, $\mathbf{J}_\star$ is the stellar angular momentum and $L(r) = r^2\Sigma\Omega$ is the disc's angular momentum per unit area. We then have,

$$N_{\rm LT} = 2\pi \sin\theta r^3 H \Sigma \Omega_{\rm LT}\Omega, \tag{48}$$

where θ is the (local) angle between $\mathbf{J}_\star$ and $\mathbf{L}$.

The LT precession is counteracted by viscosity in the disc. The associated viscous torque (along the spin axis) is,

$$N_{\rm visc} = 2\pi\nu r^3 \Sigma \Omega'. \tag{49}$$

Hereafter the disc is taken to be Keplerian, $\Omega = \Omega_{\rm K}$.

The disc is likely to undergo tearing by the precessional motion provided the LT torque exceeds the viscous torque,

$$N_{\rm LT} \gtrsim N_{\rm visc}. \tag{50}$$

For a uniform density star $J_\star = (2/5) M_\star R_\star^2 \Omega_\star$; after some straightforward algebra and with the help of the disc structure Eqs. (A1), the above inequality leads to

$$\left(\frac{r}{R_\star}\right)^{3/2} \lesssim \frac{8}{15}\sin\theta \frac{\mathcal{C}}{\alpha}\frac{\Omega_\star}{\Omega_0}\left(\frac{H}{r}\right)^{-1}, \tag{51}$$

where we have introduced the 'Kepler limit' frequency $\Omega_0 = \Omega_{\rm K}(R_\star)$ and the compactness $\mathcal{C}$ is defined in Eq. (44).

Expressing our result in terms of normalised parameters, we have

$$\frac{r}{R_\star} \lesssim 40 (\sin\theta)^{2/3} \left(\frac{\alpha}{0.1}\right)^{-2/3} \left(\frac{H/r}{10^{-3}}\right)^{-2/3} \times \nu_{500}^{2/3} M_{1.4}^{1/3} R_6^{1/3}. \tag{52}$$

For example, even a mere $\theta = 10^{\rm o}$ disc-spin misalignment would allow LT-induced tearing to take place for $r/R_\star \lesssim 12$.

So far we have ignored the presence of the stellar magnetic field. Intuitively speaking, we would expect the field lines threading the disc to resist the tearing effect of the LT torque. This argument can be quantified if we compare the LT torque with the local magnetic field torque. The latter parameter is given by $N_{\rm B} = r^3 B_\varphi B_z$ with the poloidal field given by Eq. (2). For the toroidal field we assume a functional form similar to the one of Wang (1995),

$$B_\varphi(r) = B_z(r) f(\Omega_\star/\Omega_{\rm K}). \tag{53}$$

The magnetic field would be unable to prevent the tearing of the disc when $N_{\rm LT} \gtrsim N_{\rm B}$. This condition is equivalent to

$$\left(\frac{r}{R_\star}\right)^2 \gtrsim \frac{15}{8}\frac{\alpha}{\sin\theta}\frac{H}{r}\frac{B_\star^2 R_\star}{\mathcal{C}\dot{M}\Omega_\star}|f(\Omega_\star/\Omega_{\rm K})|. \tag{54}$$

Using normalised parameters (and approximating $f \sim 1$) we obtain the following numerical estimate

$$\frac{r}{R_\star} \gtrsim 0.7 (\sin\theta)^{-1/2} \left(\frac{\alpha}{0.1}\right)^{1/2} \left(\frac{H/r}{10^{-3}}\right)^{1/2} \times B_8 R_6 M_{1.4}^{-1/2} \nu_{500}^{-1/2} \dot{M}_{-10}^{-1/2}. \tag{55}$$

This result leaves the door open for a possible LT-driven tearing of a magnetically-threaded disc. For the previous example of a $\theta = 10^{\rm o}$ misalignment (and for the rest of the parameters set to their canonical values) we find $r \gtrsim 1.7 R_\star$. Combined with the viscous upper limit (52), our estimates suggest that the LT torque could play an important role in the dynamics of the inner part of accretion discs in LMXBs.

To what extent LT precession could cause a fully nonlinear fragmentation of the disc cannot be answered by the present analysis. Numerical simulations of accreting black holes (Nixon et al. 2012; Raj & Nixon 2021) suggest that the formation of precessing 'rings' takes place above an initial misalignment $\theta \approx 50^{\rm o}$; moreover, the emergence of this structure is accompanied by a markedly enhanced accretion rate due to loss of angular momentum between the orbiting rings. Order-of-magnitude variations in $\dot{M}$ during a burst, which may not be properly accounted for when averaging in the way described in Sec. 3.1, are likely to adjust the inferred parameters of the system.

5 CONCLUSIONS

The main purpose of this paper is the comparison of the spin-up rates of a handful of AMXPs, with reliable timing data during periods of burst activity and quiescence, against a collection of theoretically predicted accretion torque models. Our results can be summarised as follows: (i) In all cases considered, none of the standard torque models endowed with magnetic field-disc coupling are able to explain the magnitude of the observed spin-up rates [in agreement with the findings of Andersson, Jones & Ho (2014)]; (ii) Thanks to their enhanced magnitude for $\xi < 1$ (where ξ is the phenomenological parameter that encapsulates much of the uncertain magnetospheric radius physics), the 'new' torques devised in this paper (see Table 1) predict spin-up rates comparable to the observed ones and at the same time are compatible with the systems' inferred dipole magnetic field strengths. Taking these results at face value we can conclude that, within the framework of standard accretion

disc physics, the observed spin-up episodes in the examined AMXPs require $\xi \approx 0.1 - 0.5$; see Figs. 3 and 6.

Moving beyond the standard accretion torque models, we have provided a quantitative analysis of the impact of some key additional physics effects. The inclusion of a quadrupole magnetic field component results in a flatter torque profile as a function of the magnetic field strength but has only a moderate effect on the maximum torque. The inclusion of GR gravity leads to moderate corrections to the disc's orbital motion (Blanchet, Faye & Ponsot 1998) and magnetospheric radius. As expected, the deviation from the Newtonian model diminishes (grows) with an increasing (decreasing) magnetic field as a result of the outwardly (inwardly) displaced magnetospheric radius. A perhaps more dramatic effect may take place, driven by the action of the LT precession torque; if sufficiently inclined, the inner part of the disc might suffer a large scale fragmentation in spite of the cohesive counter-action of the viscous and magnetic forces, leading to huge variations in $\dot{M}$ over relatively short timescales (Nixon et al. 2012; Raj & Nixon 2021).

Not surprisingly, observational errors are part of life when it comes to modelling highly transient systems like AMXPs. A case in point is SAX J1808 with its multiply inferred dipole magnetic field strength during periods of quiescence (see Fig. 7). In a similar fashion, upper limit spin-up measurements (as in the case of XTE J1814 and IGR J17494) are rather poor probes of accretion torque physics and for that reason the aforementioned systems have been omitted from our analysis. The advent of new technologies such as NICER will undoubtedly improve the quality of future timing data, and may also be able to capture the spectroscopic evolution of emission lines in bright systems, which can be used as direct and independent probes for the inner radius of the accretion disc (Papitto et al. 2009; Cackett et al. 2009).

Taking the accretion torque modelling to the next level will probably require a shift from the analytical-phenomenological models discussed here to the full armoury of 3D numerical simulations [see, e.g., Kulkarni & Romanova (2013)]. The existing MHD codes, although still limited in terms of simulation time, have now reached a point where they can evolve an accretion flow without any symmetry imposed between the spin, disc and magnetic field axes (Romanova et al. 2020). The numerical results could serve as a test of the key ingredients of the phenomenological models such as the magnetospheric radius (Kulkarni & Romanova 2013) and the functional form of the generated azimuthal magnetic field [cf. Eq. (15); (Wang 1995; Psaltis & Chakrabarty 1999)]. If robust enough, these results could be converted into analytical fit formulae and fed back into the phenomenological torque models.

ACKNOWLEDGEMENTS

AGS gratefully acknowledges financial support from the Alexander von Humboldt Foundation.

DATA AVAILABILITY STATEMENT

Observational data used in this paper are quoted from the cited works. Data generated from computations are reported in the body of the paper. Additional data can be made available upon reasonable request.

REFERENCES

Alpar M. A., Cheng A. F., Ruderman M. A., Shaham J., 1982, Nature, 300, 728
Andersson N., Glampedakis K., Haskell B., Watts A. L., 2005, MNRAS, 361, 1153
Andersson N., Jones D. I., Ho W. C. G., 2014, MNRAS, 442, 1786
Andersson N., Jones D. I., Kokkotas K. D., Stergioulas N., 2000, ApJ, 534, L75
Andersson N., Kokkotas K. D., Stergioulas N., 1999, ApJ, 516, 307
Archibald A. M. et al., 2009, Science, 324, 1411
Baglio M. C., D'Avanzo P., Muñoz-Darias T., Breton R. P., Campana S., 2013, A&A, 559, A42
Bardeen J. M., Petterson J. A., 1975, ApJL, 195, L65
Bhattacharya D., van den Heuvel E. P. J., 1991, Physics Reports, 203, 1
Bhattacharyya S., Chakrabarty D., 2017, ApJ, 835, 4
Bildsten L., 1998, ApJ, 501, L89
Bilous A. V. et al., 2019, ApJL, 887, L23
Blanchet L., Faye G., Ponsot B., 1998, Physical Review D, 58, 124002
Bogdanov S. et al., 2019, ApJL, 887, L25
Burderi L., Di Salvo T., Menna M. T., Riggio A., Papitto A., 2006, ApJL, 653, L133
Cackett E. M., Altamirano D., Patruno A., Miller J. M., Reynolds M., Linares M., Wijnands R., 2009, ApJL, 694, L21
Chakrabarty D., Morgan E. H., Muno M. P., Galloway D. K., Wijnands R., van der Klis M., Markwardt C. B., 2003, Nature, 424, 42
Choudhuri A. R., Konar S., 2002, MNRAS, 332, 933
Cumming A., Arras P., Zweibel E., 2004, ApJ, 609, 999
De Falco V., Kuiper L., Bozzo E., Galloway D. K., Poutanen J., Ferrigno C., Stella L., Falanga M., 2017, A&A, 599, A88
Doroshenko V., Suleimanov V., Tsygankov S., Mönkkönen J., Ji L., Santangelo A., 2020, A&A, 643, A62
Falanga M. et al., 2005, A&A, 444, 15
Frank J., King A., Raine D., 2002, Accretion Power in Astrophysics, 3rd edn. Cambridge University Press
Galloway D. K., Cumming A., 2006, ApJ, 652, 559
Galloway D. K., Keek L., 2021, Astrophysics and Space Science Library, 461, 209
Ghosh P., Lamb F. K., 1979, ApJ, 234, 296
Gierliński M., Poutanen J., 2005, MNRAS, 359, 1261
Gittins F., Andersson N., 2019, MNRAS, 488, 99
Gunn J. E., Ostriker J. P., 1969, Nature, 221, 454
Güver T., Özel F., 2013, ApJL, 765, L1
Hartman J. M., Patruno A., Chakrabarty D., Markwardt C. B., Morgan E. H., van der Klis M., Wijnands R., 2009, ApJ, 702, 1673
Haskell B., Patruno A., 2011, ApJL, 738, L14

Haskell B., Patruno A., 2017, Phys. Rev. Lett., 119, 161103
Ho W. C. G., Andersson N., Haskell B., 2011, Phys. Rev. Lett., 107, 101101
Keek L. et al., 2018, ApJL, 856, L37
Kluźniak W., Rappaport S. A., 2007, ApJ, 671, 1990
Krauss M. I. et al., 2005, ApJ, 627, 910
Kulkarni A. K., Romanova M. M., 2013, MNRAS, 433, 3048
Lattimer J. M., Prakash M., 2001, ApJ, 550, 426
Lattimer J. M., Steiner A. W., 2014, ApJ, 784, 123
Levin L., 1999, ApJ, 517, 328
Li X. D., Bombaci I., Dey M., Dey J., van den Heuvel E. P. J., 1999, Phys. Rev. Lett., 83, 3776
Melatos A., Payne D. J. B., 2005, ApJ, 623, 1044
Miller M. C. et al., 2021, arXiv e-prints, arXiv:2105.06979
Mukherjee D., 2017, Journal of Astrophysics and Astronomy, 38, 48
Ng M. et al., 2021, ApJL, 908, L15
Nixon C., King A., Price D., Frank J., 2012, ApJL, 757, L24
Page D., Reddy S., 2013, Phys. Rev. Lett., 111, 241102
Papitto A., Di Salvo T., D'Aì A., Iaria R., Burderi L., Riggio A., Menna M. T., Robba N. R., 2009, A&A, 493, L39
Papitto A. et al., 2013, Nature, 501, 517
Papitto A., Menna M. T., Burderi L., di Salvo T., Riggio A., 2008, MNRAS, 383, 411
Papitto A., Riggio A., Burderi L., di Salvo T., D'Aí A., Iaria R., 2011, A&A, 528, A55
Pappas G., Apostolatos T. A., 2012, Phys. Rev. Lett., 108, 231104
Patruno A., 2010, ApJ, 722, 909
Patruno A., Haskell B., Andersson N., 2017, ApJ, 850, 106
Patruno A., Watts A. L., 2021, in Timing Neutron Stars: Pulsations, Oscillations and Explosions, Belloni T. M., Méndez M., Zhang C., eds., Vol. 461, Springer Berlin Heidelberg, pp. 143–208
Pétri J., 2019, MNRAS, 485, 4573
Philippov A. A., Spitkovsky A., Cerutti B., 2015, ApJL, 801, L19
Potekhin A. Y., Chabrier G., 2018, A&A, 609, A74
Pringle J. E., Rees M. J., 1972, A&A, 21, 1
Priymak M., Melatos A., Payne D. J. B., 2011, MNRAS, 417, 2696
Psaltis D., Chakrabarty D., 1999, ApJ, 521, 332
Raj A., Nixon C. J., 2021, ApJ, 909, 82
Rappaport S. A., Fregeau J. M., Spruit H., 2004, ApJ, 606, 436
Rheinhardt M., Geppert U., 2002, Phys. Rev. Lett., 88, 101103
Riggio A., Burderi L., di Salvo T., Papitto A., D'Aì A., Iaria R., Menna M. T., 2011, A&A, 531, A140
Romanova M. M., Koldoba A. V., Ustyugova G. V., Blinova A. A., Lai D., Lovelace R. V. E., 2020, arXiv e-prints, arXiv:2012.10826
Sanna A. et al., 2017a, MNRAS, 471, 463
Sanna A. et al., 2017b, MNRAS, 466, 2910
Spitkovsky A., 2006, ApJL, 648, L51
Spruit H. C., Taam R. E., 1993, ApJ, 402, 593
Staubert R. et al., 2019, A&A, 622, A61
Strohmayer T., Mahmoodifar S., 2014, ApJL, 793, L38
Suvorov A. G., Melatos A., 2019, MNRAS, 484, 1079
Suvorov A. G., Melatos A., 2020, MNRAS, 499, 3243
Tudor V. et al., 2017, MNRAS, 470, 324
Urpin V., Geppert U., 1995, MNRAS, 275, 1117
van der Klis M., 2006, Advances in Space Research, 38, 2675
Vigelius M., Melatos A., 2009, MNRAS, 395, 1985
Wang Y.-M., 1995, ApJL, 449, L153
Wette K., Vigelius M., Melatos A., 2010, MNRAS, 402, 1099
Wijnands R., van der Klis M., 1998, Nature, 394, 344

APPENDIX A: THIN-DISC STRUCTURE EQUATIONS

This short appendix summarises the textbook equations describing the structure of the standard Shakura-Shunyaev α-viscosity thin disc model Frank, King & Raine (2002). These equations are,

$$\nu = \alpha c_s H, \quad c_s = H\Omega, \quad \Sigma = \rho H, \tag{A1}$$

where H, ρ, Σ are, respectively, the disc's thickness, density and surface density; Ω is the angular frequency, c_s is the local 'vertical' sound speed and ν is the shear viscosity coefficient. Viscosity is expressed in terms of the phenomenological α parameter.

Another key equation of the model is the relation between surface density and accretion rate:

$$\Sigma \approx \frac{\dot{M}}{3\pi\nu}. \tag{A2}$$

For a Keplerian disc, this relation allows us to express the disc's density profile as,

$$\rho(r) \approx \frac{\dot{M}}{3\pi\alpha}\left(\frac{H}{r}\right)^{-3}(GM_\star r^3)^{-1/2}. \tag{A3}$$